Associations of quantitative susceptibility mapping with Alzheimer's disease clinical and imaging markers

Petrice M. Cogswell[a,*], **Heather J. Wiste**[b], **Matthew L. Senjem**[a,c], **Jeffrey L. Gunter**[a,c], **Stephen D. Weigand**[b], **Christopher G. Schwarz**[a], **Arvin Arani**[a], **Terry M. Therneau**[b], **Val J. Lowe**[a], **David S. Knopman**[d], **Hugo Botha**[d], **Jonathan Graff-Radford**[d], **David T. Jones**[d], **Kejal Kantarci**[a], **Prashanthi Vemuri**[a], **Bradley F Boeve**[d], **Michelle M. Mielke**[b,d], **Ronald C. Petersen**[b,d], **Clifford R. Jack Jr**[a]

[a]Department of Radiology, Mayo Clinic, 200 First St SW, Rochester, MN 55905, USA

[b]Department of Health Sciences Research, Mayo Clinic, 200 First St SW, Rochester, MN 55905, USA

[c]Department of Information Technology, Mayo Clinic, 200 First St SW, Rochester, MN 55905, USA

[d]Department of Neurology, Mayo Clinic, 200 First St SW, Rochester, MN 55905, USA

Abstract

Altered iron metabolism has been hypothesized to be associated with Alzheimer's disease pathology, and prior work has shown associations between iron load and beta amyloid plaques. Quantitative susceptibility mapping (QSM) is a recently popularized MR technique to infer local tissue susceptibility secondary to the presence of iron as well as other minerals. Greater QSM values imply greater iron concentration in tissue. QSM has been used to study relationships between cerebral iron load and established markers of Alzheimer's disease, however relationships remain unclear. In this work we study QSM signal characteristics and associations between susceptibility measured on QSM and established clinical and imaging markers of Alzheimer's disease. The study included 421 participants (234 male, median age 70 years, range 34–97 years) from the Mayo Clinic Study of Aging and Alzheimer's Disease Research Center; 296 (70%) had a diagnosis of cognitively unimpaired, 69 (16%) mild cognitive impairment, and 56 (13%) amnestic dementia. All participants had multi-echo gradient recalled echo imaging, PiB amyloid PET, and Tauvid tau PET. Variance components analysis showed that variation in cortical susceptibility across participants was low. Linear regression models were fit to assess associations with regional susceptibility. Expected increases in susceptibility were found with older age and cognitive impairment in the deep and inferior gray nuclei (pallidum, putamen, substantia nigra, subthalamic nucleus) (betas: 0.0017 to 0.0053 ppm for a 10 year increase in age, $p = 0.03$ to < 0.001; betas: 0.0021 to 0.0058 ppm for a 5 point decrease in Short Test of Mental Status, $p = 0.003$ to $p < 0.001$). Effect sizes in cortical regions were smaller, and the age associations were generally

*Corresponding author. Cogswell.Petrice@mayo.edu (P.M. Cogswell).

negative. Higher susceptibility was significantly associated with higher amyloid PET SUVR in the pallidum and putamen (betas: 0.0029 and 0.0012 ppm for a 20% increase in amyloid PET, $p = 0.05$ and 0.02, respectively), higher tau PET in the basal ganglia with the largest effect size in the pallidum (0.0082 ppm for a 20% increase in tau PET, $p < 0.001$), and with lower cortical gray matter volume in the medial temporal lobe (0.0006 ppm for a 20% decrease in volume, $p = 0.03$). Overall, these findings suggest that susceptibility in the deep and inferior gray nuclei, particularly the pallidum and putamen, may be a marker of cognitive decline, amyloid deposition, and off-target binding of the tau ligand. Although iron has been demonstrated in amyloid plaques and in association with neurodegeneration, it is of insufficient quantity to be reliably detected in the cortex using this implementation of QSM.

Keywords

Quantitative susceptibility mapping; Beta amyloid PET; Tau PET; Alzheimer's disease

1.   Introduction

Altered iron metabolism has been hypothesized to be associated with Alzheimer's disease pathology, as supported by histochemical, histopathology, and imaging studies. Histochemical studies have shown accumulation of iron in brain regions with Alzheimer's disease histopathologic changes and associations with beta amyloid aggregates and neurofibrillary tangles (Deibel et al., 1996; Smith et al., 1997; Hautot et al., 2003; Collingwood et al., 2005, 2008; Everett et al., 2014). Magnetic resonance (MR) studies using ex vivo samples and an in vivo mouse model have detected iron associated with amyloid plaques based on T2* properties (Benveniste et al., 1999; Jack et al., 2004, 2005; Meadowcroft et al., 2009). More recently, it has been proposed that iron accumulation and, therefore, potentially plaque accumulation may be measured in vivo using quantitative susceptibility mapping (QSM), a non-invasive MRI technique capable of measuring tissue susceptibility from a gradient recalled multi-echo acquisition (Haacke et al., 2015; Liu et al., 2015; Wang and Liu, 2015).

Although the susceptibility measured by QSM is nonspecific and can be due to substances such as iron, calcium, lipid, or myelin, in the study of neurodegenerative diseases it is generally considered a measure of cortical iron (Li et al., 2011; Deistung et al., 2013; Lim et al., 2013). QSM signal (susceptibility) has been studied with respect to aging and cognition, as well as with amyloid PET signal. Susceptibility has been shown to increase with age in the regions of the cortex as well as deep gray nuclei (Bilgic et al., 2012; Acosta-Cabronero et al., 2016; Zhang et al., 2018). Studies have demonstrated the correlation of susceptibility with cognitive decline (van Bergen et al., 2016; Ayton et al., 2017; Kim et al., 2017; van Bergen et al., 2018) and shown differences in QSM signal between Alzheimer's disease and cognitively unimpaired participants (Acosta-Cabronero et al., 2013; Tiepolt et al., 2018). QSM has been used to study correlations between iron deposition and amyloid accumulation based on amyloid PET (van Bergen et al., 2016; Ayton et al., 2017; Tiepolt et al., 2018; van Bergen et al., 2018) and in ex vivo brain specimens and in vivo mouse models (Gong et al., 2019). However, associations between susceptibility and amyloid are variable among

studies, with some studies showing no significant association in the cortex, some showing regional positive associations, and some showing associations that depend on relative amounts of amyloid and iron. Relationships between QSM signal and established markers of neurodegeneration and Alzheimer's disease remain unclear.

The goals of this study were to (i) describe the regional and within-participant variability in susceptibility across cortical and deep and inferior gray regions as quantified by QSM, (ii) assess associations between susceptibility and clinical variables of age, cognition, and clinical diagnosis, and (iii) assess associations between susceptibility and imaging measures of amyloid PET standardized uptake value ratio (SUVR), tau PET SUVR, and cortical volume in a population of study participants with diagnoses of cognitively unimpaired (CU), mild cognitive impairment (MCI), and amnestic dementia. This study will help inform about the suitability of QSM for clinical and research applications.

2. Materials and methods

2.1. Participants, inclusion criteria

Individuals in this study were enrolled in either the Mayo Clinic Study of Aging (MCSA), a longitudinal cohort study of residents in Olmsted County, Minnesota (Roberts et al., 2008), or the Mayo Alzheimer's Disease Research Center (ADRC), a longitudinal study of patients identified through the clinical practice. This study was approved by the Mayo Clinic and Olmsted Medical Center Institutional Review Boards, all participants provided written informed consent, and the study was carried out in accordance with the Declaration of Helsinki. If participants had cognitive impairment sufficient to interfere with capacity, consent was obtained from a legally authorized representative. All participants underwent evaluation including review of past medical history, mental status examination, neurologic examination, and neuropsychological assessment. These were used to determine clinical diagnoses of MCI and dementia via expert panel review and using established criteria (Petersen, 2004; McKhann et al., 2011). Cognitively unimpaired individuals were those who did not meet criteria for either MCI or dementia.

Inclusion criteria for this study were a 3D multi-echo GRE (3D-MEGRE) MR, amyloid PET, tau PET, and clinical diagnosis of cognitively unimpaired, mild cognitive impairment, or amnestic dementia. The age ranges of this study correspond with the age ranges recruited for the MCSA and ADRC. These studies include young adults, as detecting early stages of aging requires studying this group. Similarly, iron deposition is present in young adults (Bilgic et al., 2012; Li et al., 2014). Therefore, it is reasonable to include a wide age range in this study when assessing associations between age and susceptibility.

2.2. Cognitive assessment

The Short Test of Mental Status (STMS) (Kokmen et al., 1991) was used as the measure of cognitive performance. For a small number of individuals where STMS was not available ($n = 8$), but the Montreal Cognitive Assessment (MoCA) was available, the MoCA test score was converted to an equivalent STMS test score (Townley et al., 2019). The STMS was chosen as a metric of cognition as it works across the cognitive range such that one cognitive

assessment may be used for both cognitively unimpaired and cognitively impaired participants.

2.3. T1w image acquisition and processing

MRI was performed on a 3.0T system (Siemens Prisma VE11C). T1-*weighted* (T1*w*) imaging was performed using a 3D Magnetization Prepared Rapid Acquisition Gradient Recalled Echo (MPRAGE) sequence with parameters: TR/TE ~2300/3 ms, TI 900 ms, spatial resolution $0.8 \times 0.8 \times 0.8$ mm^3. We used Unified Segmentation (Ashburner and Friston, 2005) in SPM12 with population-optimized templates and settings from the Mayo Clinic Adult Lifespan Template (MCALT: https://www.nitrc.org/projects/mcalt/). Total intracranial volume (TIV) masks were computed from these segmentations, as previously described (Schwarz et al., 2016b). The gray matter was segmented by two atlases that included the cortex and gray nuclei. The first atlas, MCALT_ADIR122 (https://www.nitrc.org/projects/mcalt/), contained 86 cortical regions-of-interest (ROIs), 43 right and 43 left, and was chosen to evaluate cortical regions in detail. The second atlas combined the ADIR122 regions in a manner similar to MCALT_ADIR28 (https://www.nitrc.org/projects/mcalt/) and contained a total of 14 cortical ROIs: frontal, parietal, temporal, medial temporal, cingulate, sensorimotor, and occipital for the left and right cerebral hemispheres. The 14 gray nuclei will be referred to as two groups, the deep and inferior gray nuclei. The deep gray nuclei included the basal ganglia (pallidum, putamen, and caudate) and thalamus. The inferior gray nuclei included the subthalamic nucleus, substantia nigra, and red nucleus. Regions are based on the DISTAL atlas (Ewert et al., 2018). The atlases contain additional cerebellar ROIs that were not used in this study.

Gray matter volumes were calculated in the cortical ROIs using the sum of probabilities computed by Unified Segmentation within each ROI. Gray matter volume analysis was not performed for the deep and inferior gray nuclei due to unreliable segmentation.

2.4. QSM image acquisition and processing

The 3D-MEGRE acquisition, from which the QSM was obtained, consisted of five echoes with acquisition parameters: TR 28 ms; TE 6.7, 10.6, 14.5, 18.4, and 22.4 ms; flip angle 15°; FOV 200×200 mm; acquired matrix 384×269; reconstructed in-plane resolution 0.52×0.52 mm^2; slice thickness 1.8 mm; slices 88; GRAPPA Ry = 2; acquisition time 6:37 min:s. These parameters and the number of echoes were chosen based on prior literature and a balance of SNR available at the last echo, bandwidth, and spatial resolution. A publically available software package (STI Suite, https://www.eecs.berkeley.edu/~chunlei.liu/software.html) was used to process the 3D-MEGRE data and generate QSM maps. First, affine registration parameters were computed between the T1*w* images and mean of the magnitude GRE images across echo times, and these were used to align the TIV mask with the magnitude and phase GRE images. Laplacian-based phase unwrapping was applied, and masking was performed to remove voxels not in the gray matter or white matter based on the T1 segmentation (Li et al., 2011; Wu et al., 2012). Finally, a sparse linear equations and least squares (LSQR) method (Li et al., 2011) was applied to compute the QSM from the unwrapped, masked phase data. Quality control was performed to assess image quality (e.g. motion artifact, susceptibility artifact obscuring parenchymal assessment) and to assess for

accurate registration of the MEGRE images to T1 space. Fifteen QSM scans were excluded due to poor image quality.

As some prior studies have used a reference region for QSM analyses, we assessed both the unnormalized and normalized QSM data. A frontal white mater ROI with a 3×3 erosion kernel was used as a reference region, as frontal white matter has been shown to be the region with the least variation in susceptibility (Ayton et al., 2017; Fazlollahi et al., 2017). The QSM signal in each ROI was calculated as the median across all voxels in that ROI; this was used for the unnormalized data analyses. The median QSM signal in the eroded frontal white matter ROI was subtracted from the median QSM signal in each ROI for the normalized data analyses. For some analyses, corresponding left and right ROIs were combined using a voxel-number weighted average of the median.

2.5. PET imaging and analysis

Amyloid PET was performed with Pittsburgh compound B (Klunk et al., 2004). Tau PET was performed with Tauvid ([18F]flortaucipir) (Avid Radiopharmaceuticals) (Schwarz et al., 2016a). Low dose CT was used for attenuation correction. PET SUVR values were determined by normalization to the cerebellar crus gray matter (Jack et al., 2017). The PET data were co-registered with the T1 w images using a rigid transformation in SPM12. Masking was performed to remove voxels not containing primarily gray or white matter by T1 segmentation. The atlas ROIs were applied to the PET SUVR data to generate region-level summary statistics for each ROI via an in-house processing pipeline (Senjem et al., 2005). Median ROI values were used for analysis and regions were combined using a voxel-number weighted average.

2.6. Statistical analysis

First, distributions and characteristics of the QSM signal were studied to inform the choice of ROIs for further analysis. Susceptibility was plotted for each cortical ROI in the ADIR122 and ADIR28 atlases as well as the deep and inferior gray nuclei to visually compare the distribution of susceptibility among participants across the regions. The ROIs in the left and right cerebral hemispheres were considered individual regions. Both the unnormalized and normalized QSM data were examined.

To better understand the sources of variability in the QSM signal, we performed a variance components analysis using linear mixed effects models where the response was median susceptibility in each region (keeping left and right sides distinct). The model included two factors of variability: region and participant. These factors were treated as random effects leading to three variance components: variability due to participant, variability due to region, and variability due to random error. Estimation was performed using restricted maximum likelihood (REML) (Pinheiro and Bates, 2000; Theory and Computational Methods for Linear Mixed-Effects Models, 2000; Cox and Solomon, 2003). The magnitudes of standard deviations (SDs) of these three variance components were compared. Because of the order-of-magnitude difference in QSM signal, we fit one model including cortical regions and a second model including deep and inferior gray nuclei. The assumption motivating these models is that while one can expect different degrees of regional variation across

biomarkers, an informative biomarker requires the participant-to-participant variation to be appreciably greater than the residual/error variation. For comparison, variance components models were performed for amyloid PET SUVR, tau PET SUVR, and cortical volume.

Pearson correlations were performed between susceptibility in the corresponding left and right ROIs to evaluate for differences between sides. Based on the results of the above analyses, further analyses were performed using the ADIR28 atlas, combining the right and left sides. This yielded a total of 14 ROIs: 7 cortical and 7 deep and inferior gray nuclei.

Associations between susceptibility as an outcome and age, STMS, clinical diagnosis, amyloid PET SUVR, tau PET SUVR, and cortical volume as predictors were assessed using linear regression models fit separately for each region. The association between age and susceptibility was estimated among MCSA participants only, as the ADRC cohort included early-onset Alzheimer's disease cases who are not representative of the typical aging spectrum. All other models were adjusted for age and sex and the models using volume as a predictor were also adjusted for TIV. We reported the following effect sizes: estimates of mean difference in susceptibility for a 10-year increase in age, a 5-point decrease/worsening in STMS, a 20% increase in amyloid PET, a 20% increase in tau PET SUVR, and a 20% decrease in gray matter volume. Additionally, estimates of mean difference in susceptibility among MCI and amnestic dementia were shown compared to cognitively unimpaired.

The linear regression models assume that susceptibility and the continuous predictors are approximately linearly related. To evaluate if the assumption was appropriate, we also fit each of the models with continuous predictors (14 age + 14 STMS + 14 amyloid PET + 14 tau PET + 7 cortical volumes = 63 models) using a 3-degree-of-freedom restricted cubic spline for the predictor to allow for nonlinearity in the relationship with susceptibility. The Bayesian Information Criteria (BIC) were compared between the spline and linear fits for each.

Associations with $p<0.05$ were considered statistically significant. All analyses were done using the R language and environment for statistical computing version 3.6.2.

2.7. Data availability

Numeric data underlying these analyses will be made available to investigators upon reasonable request.

3. Results

3.1. Participants

A total of 421 participants were included (234 male, median age 70 years, range 34–97 years); 296 (70%) had a diagnosis of cognitively unimpaired, 69 (16%) MCI, and 56 (13%) amnestic dementia. Demographics are summarized in Table 1. Imaging was performed between April 2018 and July 2019. The time between imaging exams was a median (inter-quartile range) of 1 (0, 3) days from MRI to PET.

3.2. Evaluation of regional susceptibility

Dot plots of median susceptibility across all participants in each ROI (Fig. 1 and Supplemental Fig. 1) showed that the distribution of signal among participants was similar across the cortical ROIs, with a narrow range of susceptibility among participants generally centered at or near zero. With the exception of the thalamus, the deep and inferior gray nuclei had a greater magnitude of susceptibility with a correspondingly wider range of values. When comparing plots of the ADIR122 (Supplemental Fig. 1) and ADIR28 atlases (Fig. 1), no additional information was gained with the more granular atlas, and therefore, the ADIR28 atlas was used going forward. Using the white matter reference region for normalization typically resulted in all regional values increasing by a small number but did not change the overall data distributions (Supplemental Fig. 1). Subsequent analyses were essentially unchanged with use of the reference region, and, therefore, only the results using the unnormalized data are shown.

Pearson correlations between the right and left regions in the ADIR122 atlas (Supplemental Fig. 2) showed only weak to moderate correlations between the sides. With no prior expectation of biological asymmetry, we interpreted the relatively low correlations as primarily reflecting measurement variation. Therefore, the two sides were combined for further analysis as a way to reduce random variation. Correlations between the two sides were generally higher in the deep and inferior gray regions.

While Fig. 1 indicated very little regional variability across cortical regions but a greater degree of variability across deep and inferior gray regions, it is also important to assess the extent of variation across participants. Fig. 2 and Table 2 show the results of a variance components analysis. For susceptibility in the cortical ROIs, the SD across participants was low and on the order of the regional and error SDs. In comparison, amyloid and tau PET showed a relatively large degree of variation across participants for cortical regions. For cortical volume the SD was greatest across regions given the wide range of ROI sizes. For susceptibility in the deep and inferior gray nuclei, the SD across regions was greater than that across participants and the estimated error. For amyloid PET and tau PET in the deep and inferior gray nuclei, the SDs across the three variance components were comparable.

3.3. Associations between susceptibility and demographic or clinical metrics

Associations between susceptibility and age, cognition (STMS), and diagnosis are shown in Fig. 3. Cortical and gray nuclei regions are shown separately as the cortical effect sizes are on average a factor of 10 less than deep and inferior gray nuclei effect sizes. Susceptibility in general increased with age in the deep and inferior gray nuclei with an increase ranging from 0.0017 ppm (95% CI: 0.0002–0.0032; $p = 0.03$) for a 10 year increase in age in the pallidum to 0.0053 ppm (95% CI: 0.0031–0.0075; $p<0.001$) in the subthalamic nucleus. In the thalamus, susceptibility showed a small decrease with older age (beta: −0.0014; 95% CI: −0.0018 to −0.0011; $p<0.001$). The majority of the cortical regions had a small but statistically significantly negative association between susceptibility and age. In models adjusted for age and sex, lower STMS scores (i.e. worse cognition) were associated with greater susceptibility in most deep and inferior gray nuclei, ranging from a 0.0021 ppm (95% CI: 0.0007–0.0035; $p = 0.003$) increase in the putamen for a 5 point decrease in STMS

to a 0.0058 ppm (95% CI: 0.0026–0.0091; p<0.001) increase in the substantia nigra. In the cortex, greater susceptibility was also associated with lower STMS in the occipital, parietal, and sensorimotor regions with smaller effect sizes. Relative to CU participants, participants with amnestic dementia had higher susceptibility in the occipital, parietal, sensorimotor, pallidum, substantia nigra, and subthalamic nucleus regions (effect sizes ranging from 0.0005 ppm [p = 0.01] in the occipital to 0.014 ppm [p<0.001] in the subthalamic nucleus). However, amnestic dementia participants had lower susceptibility compared to CU in the thalamus (effect size −0.0027 ppm [p<0.001]). Patients with mild cognitive impairment showed no clear pattern of differences in susceptibility compared to CU. Box plots of susceptibility by diagnosis for each region are shown in Supplemental Fig. 3.

3.4. Associations between susceptibility and imaging metrics

Associations between susceptibility and imaging metrics of amyloid PET SUVR, tau PET SUVR, and gray matter volume are shown in Fig. 4. As in Fig. 3, the cortical regions and deep and inferior gray nuclei are shown separately due to differences in effect size (deep and inferior gray nuclei > cortical regions). For amyloid PET, there were positive associations with susceptibility in the pallidum and putamen (0.0029 ppm [p = 0.05] and 0.0012 ppm [p = 0.02] increase for a 20% increase in amyloid PET, respectively) but negative associations in several regions including the frontal and temporal ROIs (−0.0001 ppm [p = 0.04] and −0.0001 [p = 0.01], respectively). Associations of susceptibility and tau PET SUVR tended to be positive with the largest association seen in the pallidum where a 20% increase in tau PET was associated with a 0.0082 ppm (95% CI: 0.0057–0.0107; p<0.001) increase in susceptibility (Fig. 4). Representative examples of the associations between susceptibility and amyloid and tau PET are shown in Fig. 5. Greater susceptibility was associated with lower cortical volume in the medial temporal region (0.0006 ppm [95% CI: 0.0001–0.0012; p = 0.03] increase for a 20% decrease in volume) with variable and non-significant relationships between susceptibility and volume in the other cortical regions.

Nonlinearity in the associations between susceptibility and age, STMS, and other imaging measures was evaluated, and both linear and nonlinear fits are shown for one cortical and one deep and inferior gray region in Supplemental Fig. 4. In 61 of the 63 models, the BIC was lower (better) for the linear vs spline fit indicating the linear model was an appropriate fit.

4. Conclusions

In this study we assessed regional and inter-participant variability in susceptibility throughout the cerebral gray matter on QSM and evaluated associations between susceptibility and clinical and imaging measures of neurodegeneration and Alzheimer's disease. The main findings were (i) participant to participant variation in QSM signal was small, which may limit ability to detect associations with other measures, (ii) there were expected increases in susceptibility with age and cognitive decline in the deep and inferior gray nuclei with smaller, more variable associations in cortical regions, (iii) susceptibility was positively associated with amyloid PET SUVR in the basal ganglia with small negative associations in some cortical regions, (iv) susceptibility was positively associated with tau

PET SUVR in the deep and inferior gray and to a lesser extent the cortical regions, and (v) only the medial temporal regions showed a small association between susceptibility and cortical volume.

Corresponding with known regions of iron deposition, susceptibility was much greater (by approximately a factor of 10) in the basal ganglia and inferior gray nuclei than in cortical regions. A clinically useful biomarker should have much greater inter-person variance across a phenotypically diverse cohort in comparison to the estimated inherit measurement error. However, in both the cortical and deep and inferior gray nuclei, the participant to participant variation in susceptibility was small and of a similar magnitude as the error SD, which may limit our ability to detect associations between the QSM measure and other imaging or clinical measures. The limited inter-person variability in susceptibility contrasts with that of established Alzheimer's disease imaging biomarkers of amyloid and tau PET, which have a relatively large variance among participants relative to regional differences and error. Although the study designs are different, we note that our estimates of error in susceptibility are comparable to previously published estimates (Deh et al., 2015; Hinoda et al., 2015).

We evaluated differences in signal among cortical ROIs and between corresponding right and left regions using a more granular cortical parcellation (ADIR122 atlas) but found it did not provide additional information in comparison to the coarser parcellation of the ADIR28 atlas. The smaller ROIs may be more susceptible to noise and, therefore, the larger ROIs of the ADIR28 atlas were chosen for subsequent analyses. Similarly, corresponding right and left ROIs showed no systematic difference and, therefore, right and left sides were combined. As smaller ROIs may be more specific for detection of MCI or dementia, the subsectioning of lobes in the ADIR28 atlas was chosen in an attempt to preserve some regional specificity, for example with a medial temporal lobe region.

Susceptibility and age were positively associated in the pallidum, putamen, subthalamic nuclei, and substantia nigra. These findings correspond with known age-related iron deposition in these regions and have been similarly demonstrated in prior QSM studies (Bilgic et al., 2012; Li et al., 2014; Acosta-Cabronero et al., 2016). We predicted that susceptibility would similarly increase with age in the cortical regions in association with iron deposition and neurodegeneration, as some of the prior QSM studies have shown (Li et al., 2014; Acosta-Cabronero et al., 2016). However, in our study, cortical regions showed variable results with very small, yet statistically significant, negative associations in most regions, particularly in the cingulate and medial temporal regions. Given the small effect sizes, findings may not be clinically meaningful and are of unclear etiology. The difference among results in the cortical regions and lack of anticipated increase in cortical susceptibility with age may be due to differences in study population and ROI selection. Measured susceptibility in cortical regions that include all cortical layers, as in this study, reflects cumulative effects of regional iron and myelin, which have been shown to both be of highest concentration in the deeper cortical layers and vary in relative amounts across the cerebral cortex (Duyn et al., 2007). While ex vivo studies may allow iron and myelin effects to be separately studied, current in vivo techniques do not allow for such distinction.

Overall, cortical and deep and inferior gray regions showed an expected increase in susceptibility with declining STMS and with a diagnosis of dementia vs cognitively unimpaired. STMS showed a larger association with susceptibility in the pallidum, putamen, substantia nigra, and subthalamic nuclei. As described above, these greater effect sizes in the deep and inferior nuclei are likely based on the greater dynamic range in these regions. Prior studies have similarly shown an increase in susceptibility, presumably iron deposition, with a decrease in cognition and diagnosis of dementia vs cognitively unimpaired that is greater in the deep gray nuclei than cortex (Ayton et al., 2017; Kim et al., 2017; Tiepolt et al., 2018).

As with the clinical associations, QSM showed larger effect sizes with other imaging markers in the deep and inferior gray nuclei than in cortical regions. Susceptibility and amyloid PET showed positive associations in the pallidum and putamen independent from age and sex; prior work has similarly shown the greatest correlation of amyloid PET and susceptibility in the basal ganglia (van Bergen et al., 2018). Relationships between cortical susceptibility and amyloid have been more variable in the literature, with some prior work identifying positive correlations between susceptibility and amyloid PET in the frontotemporal cortex (Ayton et al., 2017; van Bergen et al., 2018) and others finding no significant relationships (Tiepolt et al., 2018). In this study relationships between cortical susceptibility and amyloid PET SUVR were variable. Statistically significant negative associations of susceptibility and amyloid in the frontal and temporal lobes had small effect sizes, –0.0001 compared to 0.0012 in the putamen. Our findings suggest that although cortical iron has been found to be associated with beta amyloid plaques in ex vivo and animal studies, it does not appear to be of sufficient quantity for in vivo detection on QSM. Alternatively, the iron associated with plaques may not demonstrate the anticipated paramagnetic properties, or there may be counteracting regional diamagnetic effects. While recent ex vivo works suggest that the negative associations of susceptibility and amyloid in some cortical ROIs may reflect amyloid deposition without localization of iron (Gong et al., 2019), prior studies have indicated that iron facilitates, and may be necessary for, amyloid plaque formation (Huang et al., 1999; Telling et al., 2017).

Associations between QSM and tau PET have been less extensively studied. We found a positive association between susceptibility and tau PET SUVR in the basal ganglia and saw a similar pattern in the cortical regions. Associations of tau PET and susceptibility are most likely due to off-target binding of the tau ligand, as similarly suggested in prior literature demonstrating correlations of tau PET SUVR and susceptibility in the basal ganglia and cortex (Choi et al., 2018; Spotorno et al., 2020). Off-target tau binding may be secondary to monoamine oxidase (MAO) and/or iron deposition in the setting of inflammation, as has been shown to occur with multiple tau tracers and confirmed with autopsy studies (Harada et al., 2018; Lemoine et al., 2018; Baker et al., 2019). Though not quantified, the extent of elevated susceptibility and tau PET SUVR do not appear to exactly overlap on visual inspection (Fig. 5B). Findings suggest the possibility of two physiologic processes in basal ganglia that may not be related to each other on a voxel-wise basis. Further study of tau PET ligands in the basal ganglia may help better understand the relationship of susceptibility changes with off-target tau binding.

The medial temporal lobe was the only cortical region to show a statistically significant increase in susceptibility with a decrease in cortical volume. This finding may represent iron deposition associated with neurodegeneration. However, given the small effect size and relatively wide confidence interval, partial volume effects in the medial temporal lobe are also possible. The lack of significant associations between gray matter volume and susceptibility in the remainder of the cortical regions is in agreement with prior work (van Bergen et al., 2018).

As described with respect to each of the clinical and imaging variables evaluated, results of QSM studies in respect to Alzheimer's disease and neurodegeneration have been variable in the cortex with more reproducible results in the deep and inferior gray nuclei. The greater dynamic range and greater regional variability in the deep and inferior gray nuclei regions relative to the cortical regions may contribute to more reliable signal and reproducible results across studies. This is best demonstrated in amyloid PET where associations of susceptibility/iron deposition and amyloid have been proven in ex vivo studies but are difficult to reproduce in in vivo human studies. Differences among study results may be due to patient population, including disease status, age, and sample size. The sample in this study is larger than that included in prior work and encompasses the spectrum from cognitively unimpaired to dementia. Differences in technique must also be considered. Acquisition parameters, such as the chosen echo times, may affect the calculated susceptibility (Sood et al., 2017). The QSM processing technique utilized in this study (STI Suite) is widely used and accepted for QSM processing. However, differences in QSM may arise from the degree of masking applied, use of or choice of a reference region, region-based vs voxel-based analysis, correction for age and other variables, and use of mean or median susceptibility. Regarding masking and noise levels, as discussed in prior studies, more advanced methods to address noise in QSM, such as adjacent to vessels or at edges of the field-of-view (e.g. anterior and middle cranial fossa) could improve the ability to detect signal in cortical regions (Acosta-Cabronero et al., 2018). The masking applied in this study should remove nearly all voxels not containing primarily parenchyma. Additionally, the use of median for our analyses should minimize effects from outlier values at edges. Therefore, more advanced methods of masking may not significantly change overall results. Regarding use of a reference region, we found similar results with vs without normalization to a reference region. In theory, normalization should not be required for QSM given that it is designed to quantify magnetic susceptibility and provide signal linearly proportional to susceptibility. Subtracting the susceptibility of a reference region would be beneficial to remove systematic variation that is larger than biologic variability in the reference region. However, if biologic changes are present in the reference region, the normalization may transfer biologic effects of the reference to other locations and confound analyses. In light of these considerations and the large size of our sample, we chose to focus our analyses on the unnormalized QSM data.

There are limitations in this study. The sample in this study is large relative to prior studies of QSM. However, the number of cognitively impaired (MCI and dementia) individuals in the sample is moderate. Additionally, because the minimum age was 34 years we were not able to asses QSM changes associated with brain development. Voxel-wise analysis was not performed; based on noise and error levels in the regional analyses it was concluded that

voxel-wise analysis would not provide additional information, particularly for cortical regions. As discussed above, cortical ROIs include all layers of the cortex, which may contain myelin, amyloid, and tau in addition to iron, and therefore observed susceptibility represents the cumulative effects of these components.

In conclusion, in this study we found regional associations of susceptibility with aging, cognition, amyloid PET, and tau PET in the basal ganglia and inferior gray nuclei. However, the cortical regions did not consistently show significant disease related changes on in vivo QSM. The variable and low level associations of cortical susceptibility with age and measures of cortical amyloid deposition and neurodegeneration appear to in part be due to inadequate biological signal and possibly inability to study individual cortical layers with QSM as currently applied. Our findings suggest that iron levels associated with cortical amyloid plaque and neurodegeneration are of insufficient quantity to be detected in vivo with QSM or that there may be local factors, including amyloid deposition, counteracting the anticipated susceptibility changes from local iron deposition. Further studies correlating in vivo imaging measures with both histopathology and ex vivo imaging may help better elucidate local susceptibility changes in neurodegeneration as well as the potential applications for QSM in assessing pathology in vivo. Overall, our findings suggest that QSM may be an informative marker in the deep and inferior gray nuclei but in the current implementation has a limited role in the cortex for clinical evaluation along the aging to dementia spectrum.

Supplementary Material

Refer to Web version on PubMed Central for supplementary material.

Acknowledgements

Abbreviations:

ADRC	Mayo Alzheimer's Disease Research Center
aDem	amnestic dementia
CU	cognitively unimpaired
MCI	mild cognitive impairment
MCSA	Mayo Clinic Study of Aging
QSM	quantitative susceptibility mapping
SUVR	standardized uptake value ratio

References

Acosta-Cabronero J, Betts MJ, Cardenas-Blanco A, Yang S, Nestor PJ, 2016 In vivo MRI mapping of brain iron deposition across the adult lifespan. J. Neurosci. Off. J. Soc. Neurosci 36, 364–374.

Acosta-Cabronero J, Milovic C, Mattern H, Tejos C, Speck O, Callaghan MF, 2018 A robust multi-scale approach to quantitative susceptibility mapping. Neuroimage 183, 7–24. [PubMed: 30075277]

Acosta-Cabronero J, Williams GB, Cardenas-Blanco A, Arnold RJ, Lupson V, Nestor PJ, 2013 In vivo quantitative susceptibility mapping (QSM) in Alzheimer's disease. PLoS One 8, e81093. [PubMed: 24278382]

Ashburner J, Friston KJ, 2005 Unified segmentation. Neuroimage 26, 839–851. [PubMed: 15955494]

Ayton S, Fazlollahi A, Bourgeat P, Raniga P, Ng A, Lim YY, et al., 2017 Cerebral quantitative susceptibility mapping predicts amyloid-β-related cognitive decline. Brain J. Neurol 140, 2112–2119.

Baker SL, Harrison TM, Maass A, Joie RL, Jagust WJ, 2019 Effect of off-target binding on 18F-flortaucipir variability in healthy controls across the life span. J. Nucl. Med 60, 1444–1451. [PubMed: 30877180]

Benveniste H, Einstein G, Kim KR, Hulette C, Johnson GA, 1999 Detection of neuritic plaques in Alzheimer's disease by magnetic resonance microscopy. Proc. Natl. Acad. Sci. U. S. A 96, 14079–14084. [PubMed: 10570201]

van Bergen JMG, X L.i., Hua J, Schreiner SJ, Steininger SC, Quevenco FC, et al., 2016 Colocalization of cerebral iron with amyloid beta in mild cognitive impairment. Sci. Rep 6, 1–9. [PubMed: 28442746]

van Bergen JMG, Li X, Quevenco FC, Gietl AF, Treyer V, Meyer R, et al., 2018 Simultaneous quantitative susceptibility mapping and Flutemetamol-PET suggests local correlation of iron and β-amyloid as an indicator of cognitive performance at high age. Neuroimage 174, 308–316. [PubMed: 29548847]

Bilgic B, Pfefferbaum A, Rohlfing T, Sullivan EV, Adalsteinsson E, 2012 MRI estimates of brain iron concentration in normal aging using quantitative susceptibility mapping. Neuroimage 59, 2625–2635. [PubMed: 21925274]

Choi JY, Cho H, Ahn SJ, Lee JH, Ryu YH, Lee MS, et al., 2018 Off-target 18F-AV-1451 binding in the basal ganglia correlates with age-related iron accumulation. J. Nucl. Med 59, 117–120. [PubMed: 28775201]

Collingwood JF, Chong RKK, Kasama T, Cervera-Gontard L, Dunin-Borkowski RE, Perry G, et al., 2008 Three-dimensional tomographic imaging and characterization of iron compounds within Alzheimer's plaque core material. J. Alzheimers Dis 14, 235–245. [PubMed: 18560134]

Collingwood JF, Mikhaylova A, Davidson M, Batich C, Streit WJ, Terry J, et al., 2005 In situ characterization and mapping of iron compounds in Alzheimer's disease tissue. J. Alzheimers Dis 7, 267–272. [PubMed: 16131727]

Cox DR, Solomon PJ.., 2003 Components of Variance [Internet]. Chapman & Hall/CRC, Boca Raton, Fla [cited 2020 Aug 15] Available from http://search.ebscohost.com/login.aspx?direct=true&scope=site&db=nlebk&db=nlabk&AN=1802301.

Deh K, Nguyen TD, Eskreis-Winkler S, Prince MR, Spincemaille P, Gauthier S, et al., 2015 Reproducibility of quantitative susceptibility mapping in the brain at two field strengths from two vendors. J. Magn. Reson. Imaging JMRI 42, 1592–1600. [PubMed: 25960320]

Deibel MA, Ehmann WD, Markesbery WR, 1996 Copper, iron, and zinc imbalances in severely degenerated brain regions in Alzheimer's disease: possible relation to oxidative stress. J. Neurol. Sci 143, 137–142. [PubMed: 8981312]

Deistung A, Schäfer A, Schweser F, Biedermann U, Turner R, Reichenbach JR, 2013 Toward in vivo histology: a comparison of quantitative susceptibility mapping (QSM) with magnitude-, phase-, and R2*-imaging at ultra-high magnetic field strength. Neuroimage 65, 299–314. [PubMed: 23036448]

Duyn JH, van Gelderen P, Li T−Q, de Zwart JA, Koretsky AP, Fukunaga M, 2007 High-field MRI of brain cortical substructure based on signal phase. Proc. Natl. Acad. Sci. U. S. A 104, 11796–11801. [PubMed: 17586684]

Everett J, Céspedes E, Shelford LR, Exley C, Collingwood JF, Dobson J, et al., 2014 Ferrous iron formation following the co-aggregation of ferric iron and the Alzheimer's disease peptide β-amyloid (1–42). J. R. Soc. Interface 11, 20140165. [PubMed: 24671940]

Ewert S, Plettig P, Li N, Chakravarty MM, Collins DL, Herrington TM, et al., 2018 Toward defining deep brain stimulation targets in MNI space: a subcortical atlas based on multimodal MRI, histology and structural connectivity. Neuroimage 170, 271–282. [PubMed: 28536045]

Fazlollahi A, Ayton S, Diouf I, Bourgeat P, Raniga P, Dore V, et al., 2017 Quantitative susceptibility mapping of the hippocampus predicts hippocampal atrophy in Aβ+ elderly controls and Alzheimer's disease patients. Alzheimers Dement J. Alzheimers Assoc 13, P454–P455.

Gong N−J, Dibb R, Bulk M, van der Weerd L, Liu C, 2019 Imaging beta amyloid aggregation and iron accumulation in Alzheimer's disease using quantitative susceptibility mapping MRI. Neuroimage 191, 176–185. [PubMed: 30739060]

Haacke EM, Liu S, Buch S, Zheng W, Wu D, Ye Y, 2015 Quantitative susceptibility mapping: current status and future directions. Magn. Reson. Imaging 33, 1–25.

Harada R, Ishiki A, Kai H, Sato N, Furukawa K, Furumoto S, et al., 2018 Correlations of 18F-THK5351 PET with postmortem burden of tau and astrogliosis in Alzheimer disease. J. Nucl. Med. Off. Publ. Soc. Nucl. Med 59, 671–674.

Hautot D, Pankhurst QA, Khan N, Dobson J, 2003 Preliminary evaluation of nanoscale biogenic magnetite in Alzheimer's disease brain tissue. Proc. R. Soc. B Biol. Sci 270, S62–S64.

Hinoda T, Fushimi Y, Okada T, Fujimoto K, Liu C, Yamamoto A, et al., 2015 Quantitative susceptibility mapping at 3 T and 1.5 T: evaluation of consistency and reproducibility. Invest. Radiol 50, 522–530. [PubMed: 25900085]

Huang X, Atwood CS, Hartshorn MA, Multhaup G, Goldstein LE, Scarpa RC, et al., 1999 The A β peptide of Alzheimer's disease directly produces hydrogen peroxide through metal ion reduction. Biochemistry 38, 7609–7616. [PubMed: 10386999]

Jack CR, Garwood M, Wengenack TM, Borowski B, Curran GL, Lin J, et al., 2004 In vivo visualization of Alzheimer's amyloid plaques by magnetic resonance imaging in transgenic mice without a contrast agent. Magn. Reson. Med 52, 1263–1271. [PubMed: 15562496]

Jack CR, Wengenack TM, Reyes DA, Garwood M, Curran GL, Borowski BJ, et al., 2005 In vivo magnetic resonance microimaging of individual amyloid plaques in Alzheimer's transgenic mice. J. Neurosci 25, 10041–10048. [PubMed: 16251453]

Jack CR, Wiste HJ, Weigand SD, Therneau TM, Lowe VJ, Knopman DS, et al., 2017 Defining imaging biomarker cut points for brain aging and Alzheimer's disease. Alzheimers Dement J. Alzheimers Assoc 13, 205–216.

Kim H–G, Park S, Rhee HY, Lee KM, Ryu C–W, Rhee SJ, et al., 2017 Quantitative susceptibility mapping to evaluate the early stage of Alzheimer's disease. NeuroImage Clin 16, 429–438. [PubMed: 28879084]

Klunk WE, Engler H, Nordberg A, Wang Y, Blomqvist G, Holt DP, et al., 2004 Imaging brain amyloid in Alzheimer's disease with Pittsburgh compound-B. Ann. Neurol 55, 306–319. [PubMed: 14991808]

Kokmen E, Smith GE, Petersen RC, Tangalos E, Ivnik RC, 1991 The short test of mental status. Correlations with standardized psychometric testing. Arch. Neurol 48, 725–728. [PubMed: 1859300]

Lemoine L, Leuzy A, Chiotis K, Rodriguez-Vieitez E, Nordberg A, 2018 Tau positron emission tomography imaging in tauopathies: the added hurdle of off-target binding. Alzheimers Dement Diagn. Assess. Dis. Monit 10, 232–236.

Li W, Wu B, Batrachenko A, Bancroft-Wu V, Morey RA, Shashi V, et al., 2014 Differential developmental trajectories of magnetic susceptibility in human brain gray and white matter over the lifespan. Hum. Brain Mapp 35, 2698–2713. [PubMed: 24038837]

Li W, Wu B, Liu C, 2011 Quantitative susceptibility mapping of human brain reflects spatial variation in tissue composition. Neuroimage 55, 1645–1656. [PubMed: 21224002]

Lim IAL, Faria AV, Li X, Hsu JTC, Airan RD, Mori S, et al., 2013 Human brain atlas for automated region of interest selection in quantitative susceptibility mapping: application to determine iron content in deep gray matter structures. Neuroimage 82, 449–469. [PubMed: 23769915]

Liu C, Li W, Tong KA, Yeom KW, Kuzminski S, 2015 Susceptibility-weighted imaging and quantitative susceptibility mapping in the brain. J. Magn. Reson. Imaging 42, 23–41. [PubMed: 25270052]

McKhann GM, Knopman DS, Chertkow H, Hyman BT, Jack CR, Kawas CH, et al., 2011 The diagnosis of dementia due to Alzheimer's disease: recommendations from the National Institute on Aging-Alzheimer's association workgroups on diagnostic guidelines for Alzheimer's disease. Alzheimers Dement J. Alzheimers Assoc 7, 263–269.

Meadowcroft MD, Connor JR, Smith MB, Yang QX, 2009 MRI and histological analysis of beta-amyloid plaques in both human Alzheimer's disease and APP/PS1 transgenic mice. J. Magn. Reson. Imaging 29, 997–1007. [PubMed: 19388095]

Petersen RC.., 2004 Mild cognitive impairment as a diagnostic entity. J. Intern. Med 256, 183–194. [PubMed: 15324362]

Pinheiro JC, Bates DM, 2000 Theory and Computational Methods for Linear Mixed–Effects Models Mixed-Effects Models in S and S-PLUS. Springer, New York, NY, pp. 57–96.

Roberts RO, Geda YE, Knopman DS, Cha RH, Pankratz VS, Boeve BF, et al., 2008 The Mayo clinic study of aging: design and sampling, participation, baseline measures and sample characteristics. Neuroepidemiology 30, 58–69. [PubMed: 18259084]

Schwarz AJ, Yu P, Miller BB, Shcherbinin S, Dickson J, Navitsky M, et al., 2016a Regional profiles of the candidate tau PET ligand 18F-AV-1451 recapitulate key features of Braak histopathological stages. Brain J. Neurol. 139, 1539–1550.

Schwarz CG, Gunter JL, Wiste HJ, Przybelski SA, Weigand SD, Ward CP, et al., 2016b A large-scale comparison of cortical thickness and volume methods for measuring Alzheimer's disease severity. NeuroImage Clin 11, 802–812. [PubMed: 28050342]

Senjem ML, Gunter JL, Shiung MM, Petersen RC, Jack CR, 2005 Comparison of different methodological implementations of voxel-based morphometry in neurodegenerative disease. Neuroimage 26, 600–608. [PubMed: 15907317]

Smith MA, Harris PLR, Sayre LM, Perry G, 1997 Iron accumulation in Alzheimer disease is a source of redox-generated free radicals. Proc. Natl. Acad. Sci. U. S. A 94, 9866–9868. [PubMed: 9275217]

Sood S, Urriola J, Reutens D, O'Brien K, Bollmann S, Barth M, et al., 2017 Echo time-dependent quantitative susceptibility mapping contains information on tissue properties. Magn. Reson. Med 77, 1946–1958. [PubMed: 27221590]

Spotorno N, Acosta-Cabronero J, Stomrud E, Lampinen B, Strandberg OT, van Westen D, et al., 2020 Relationship between cortical iron and tau aggregation in Alzheimer's disease. Brain 143, 1341–1349. [PubMed: 32330946]

Telling ND, Everett J, Collingwood JF, Dobson J, van der Laan G, Gallagher JJ, et al., 2017 Iron biochemistry is correlated with amyloid plaque morphology in an established mouse model of Alzheimer's disease. Cell Chem. Biol 24, 1205–1215. [PubMed: 28890316]

Tiepolt S, Schäfer A, Rullmann M, Roggenhofer E, Gertz H-J, et al. Netherlands Brain Bank, 2018 Quantitative susceptibility mapping of Amyloid-β aggregates in Alzheimer's disease with 7T MR J. Alzheimers Dis. JAD 64, 393–404. [PubMed: 29865069]

Townley RA, Syrjanen JA, Botha H, Kremers WK, Aakre JA, Fields JA, et al., 2019 Comparison of the Short Test of Mental Status and the Montreal Cognitive Assessment Across the Cognitive Spectrum. Mayo Clin. Proc 94, 1516–1523. [PubMed: 31280871]

Wang Y, Liu T, 2015 Quantitative susceptibility mapping (QSM): decoding MRI data for a tissue magnetic biomarker. Magn. Reson. Med 73, 82–101. [PubMed: 25044035]

Wu B, Li W, Guidon A, Liu C, 2012 Whole brain susceptibility mapping using compressed sensing. Magn. Reson. Med 67, 137–147. [PubMed: 21671269]

Zhang Y, Wei H, Cronin MJ, He N, Yan F, Liu C, 2018 Longitudinal atlas for normative human brain development and aging over the lifespan using quantitative susceptibility mapping. Neuroimage 171, 176–189. [PubMed: 29325780]
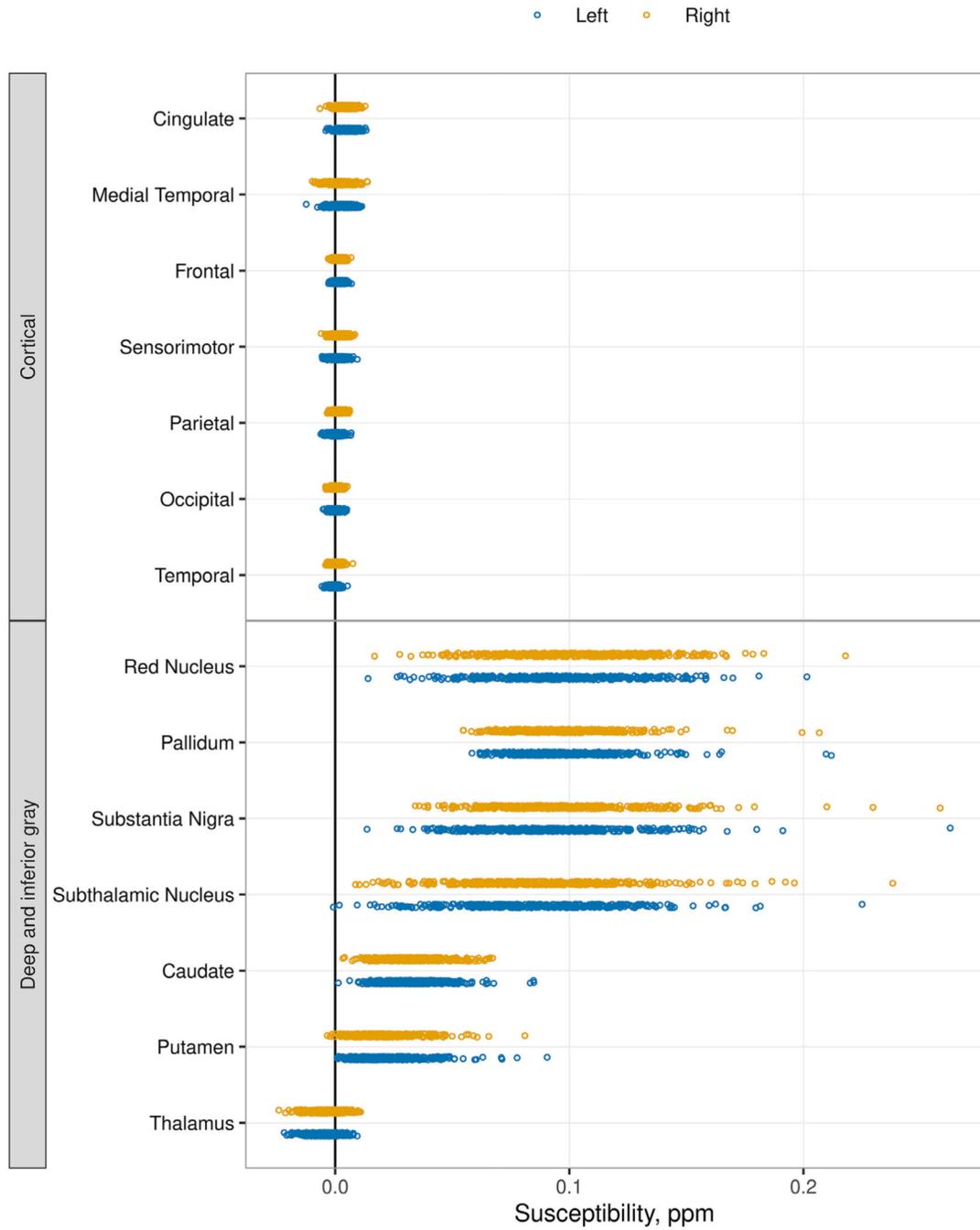
Fig. 1.
Median susceptibility by region using the ADIR28 atlas. The unnormalized QSM data are shown. For each region, each participant is represented by a dot, blue for left and orange for right. The ROIs are listed from high to low median value. The basal ganglia and inferior gray nuclei show positive susceptibility with a broad range among participants compared to the cortical ROIs, which show signal centered about zero with a relatively narrow range.
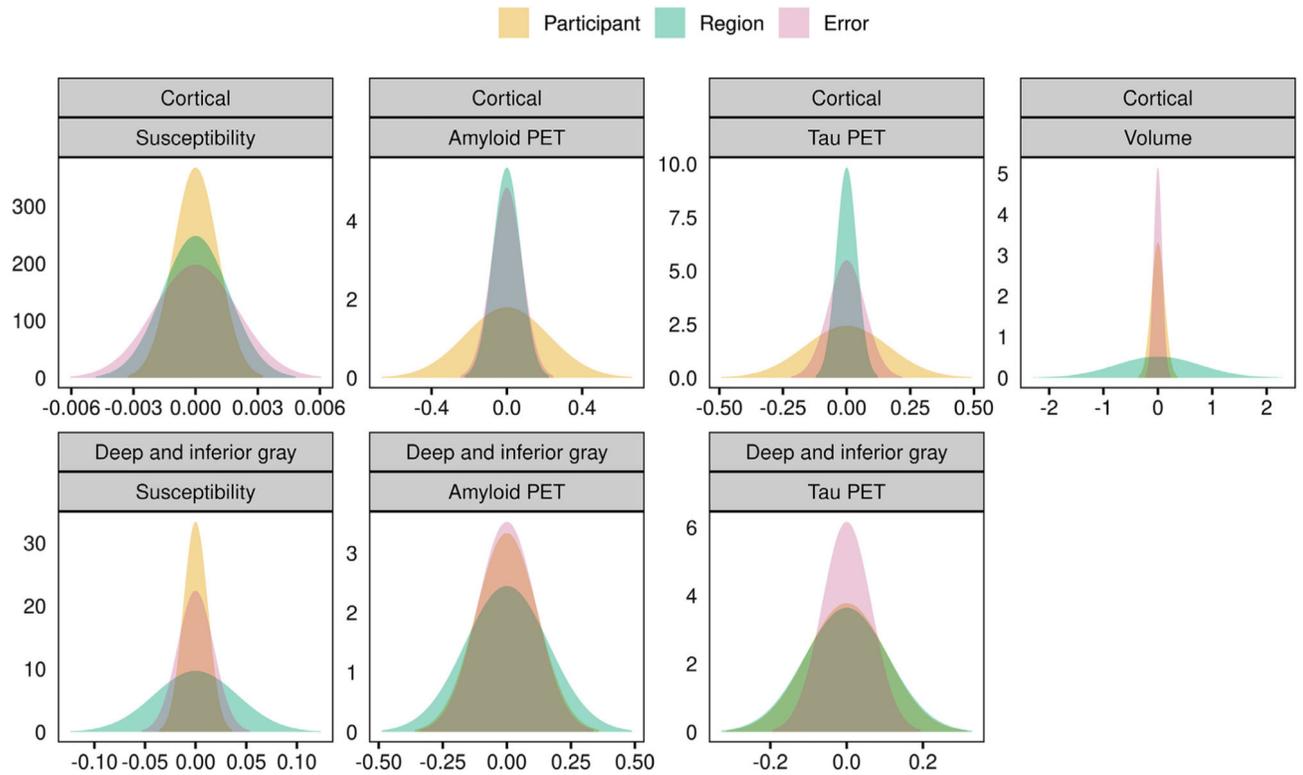
Fig. 2.
Normal densities reflecting the estimated SDs from the variance components analysis for susceptibility, amyloid PET SUVR, tau PET SUVR, and cortical gray matter volume. Analysis was performed using the unnormalized susceptibility measures and PET and volume measures were log-transformed. Results are shown separately for cortical (top row) and deep and inferior gray nuclei (bottom row). The x-axis differs among plots and is representative of spread or variation in values. The y-axis represents amplitude with values based on the SD of each measure such that the area under the curve is equal to 1.
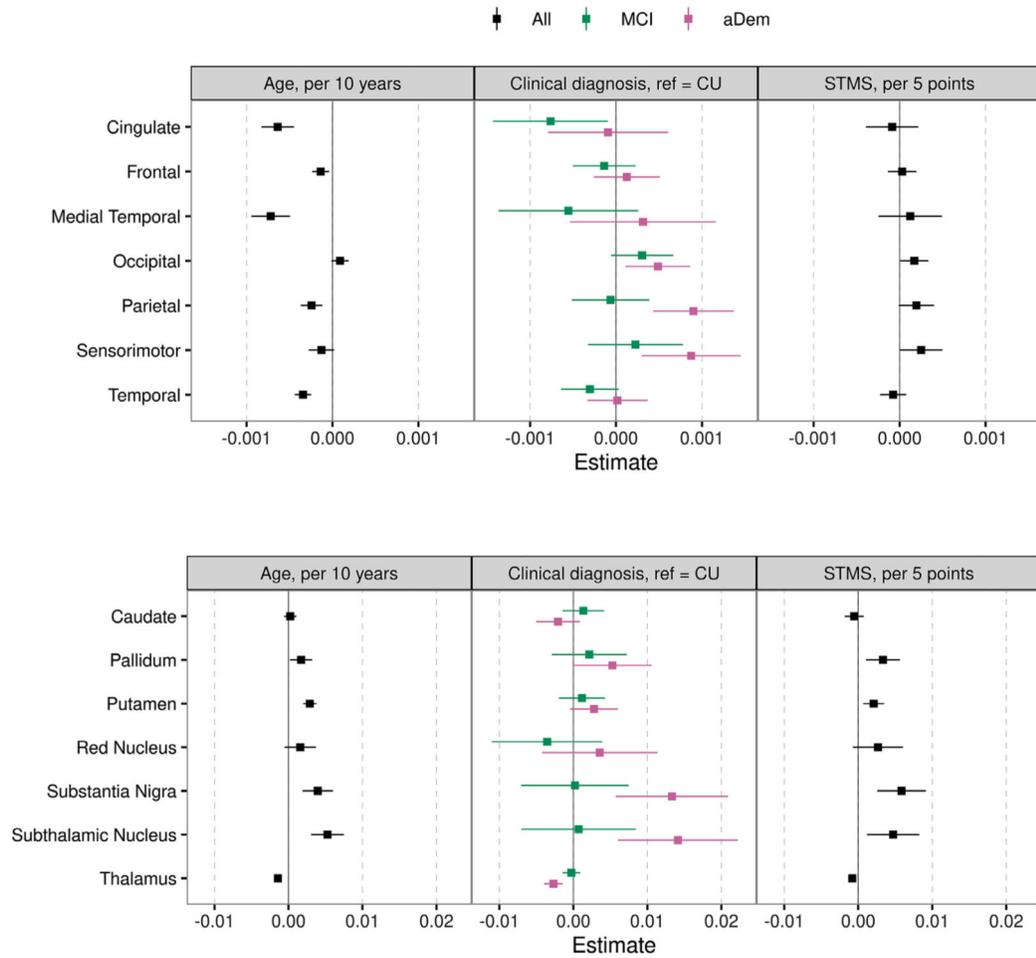
Fig. 3.
Estimated mean (95% confidence interval) difference in susceptibility for an increase in age of 10 years, diagnosis of amnestic dementia (aDem) or mild cognitive impairment (MCI) relative to cognitively unimpaired (CU), and a decrease in Short Test of Mental Status (STMS) score of 5 points. Linear regression models were fit separately for each region and variable of interest. All models except age were adjusted for age and sex. All age models were fit among MCSA participants only. Cortical regions and deep and inferior gray nuclei are shown separately due to differences in effect sizes. Those regions whose 95% confidence interval does not cross zero are statistically significant.
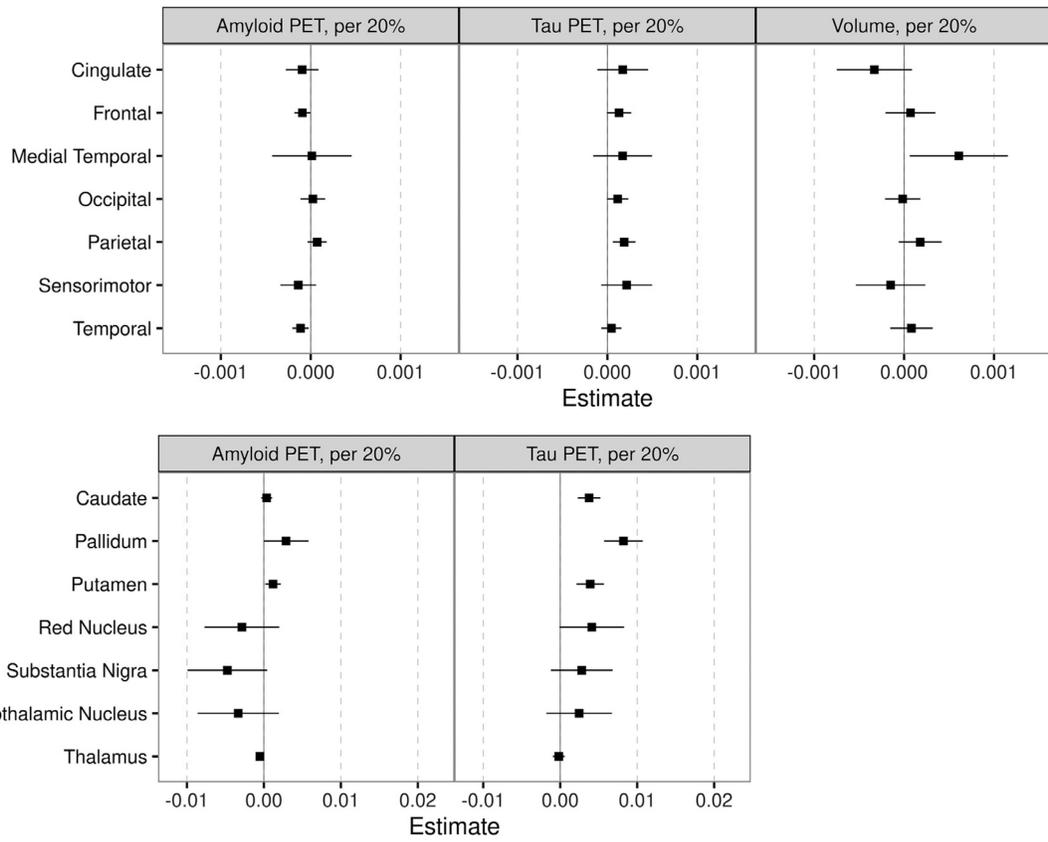
Fig. 4.
Estimated mean (95% confidence interval) difference in susceptibility for a 20% increase in amyloid PET SUVR, 20% increase in tau PET SVUR, and a 20% decrease in gray matter volume. Linear regression models were fit separately for each region and variable of interest. All models were adjusted for age and sex, and volume models were adjusted for TIV. Cortical regions and deep and inferior gray nuclei are shown separately due to differences in effect sizes. Those regions whose 95% confidence interval does not cross zero are statistically significant.
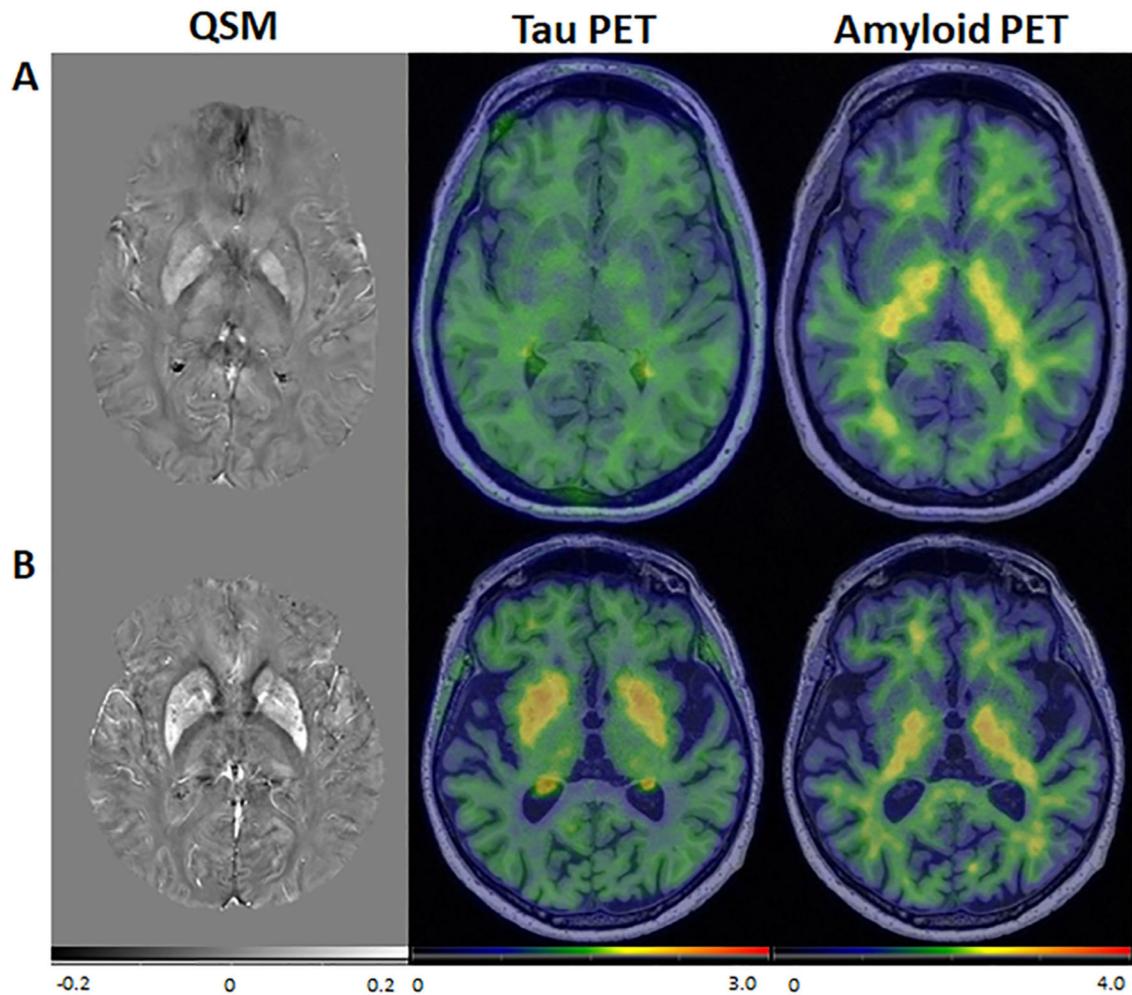
Fig. 5.
Images from representative participants. QSM, tau PET, and amyloid PET for (A) a 35-year-old participant and (B) an 83-year-old participant, both cognitively unimpaired. In the older participant, there was elevated susceptibility and tau PET SUVR in the pallidum and putamen. Though not quantified, the extent of elevated susceptibility and tau PET SUVR do not appear to exactly overlap on visual inspection, which may imply more than one process contributes to these signal changes on QSM and PET. Amyloid PET SUVR was low throughout for both of the participants.

Table 1:

Demographic characteristics of the study participants.

Characteristic	All (*N* = 421)	CU (*N* = 296)	MCI (*N* = 69)	aDem (*N* = 56)
Study, no. (%)				
MCSA	331 (79%)	280 (95%)	47 (68%)	4 (7%)
ADRC	90 (21%)	16 (5%)	22 (32%)	52 (93%)
Age, years				
Median (IQR)	70 (61, 78)	69 (59, 76)	77 (72, 86)	68 (61, 77)
Min, Max	34, 97	34, 90	46, 97	53, 89
Sex, no. (%)				
Female	187 (44%)	128 (43%)	30 (43%)	29 (52%)
Male	234 (56%)	168 (57%)	39 (57%)	27 (48%)
Education, years				
Median (IQR)	16 (13, 17)	16 (14, 17)	15 (12, 16)	16 (13, 16)
Min, Max	0, 25	8, 20	0, 21	12, 25
APOE genotype, no. (%) [*]				
*ε*4 non-carrier	261 (66%)	202 (72%)	44 (69%)	15 (29%)
*ε*4 carrier	134 (34%)	77 (28%)	20 (31%)	37 (71%)
Short Test of Mental Status				
Median (IQR)	36 (33, 37)	37 (36, 38)	32 (29, 33)	22 (18, 28)
Min, Max	5, 38	29, 38	24, 37	5, 36
Amyloid PET, SUVR [†]				
Median (IQR)	1.43 (1.33, 1.99)	1.38 (1.31, 1.49)	1.93 (1.40, 2.33)	2.40 (2.17, 2.70)
Min, Max	1.11, 3.63	1.11, 3.63	1.22, 3.30	1.46, 3.41
Abnormal, no. (%)	178 (42%)	77 (26%)	46 (67%)	55 (98%)
Tau PET, SUVR [†]				
Median (IQR)	1.20 (1.15, 1.29)	1.18 (1.14, 1.23)	1.25 (1.19, 1.38)	1.94 (1.55, 2.32)
Min, Max	0.94, 3.13	0.94, 1.57	0.99, 2.27	1.09, 3.13
Abnormal, no. (%)	138 (33%)	55 (19%)	32 (46%)	51 (91%)

[*]
APOE genotype was missing for 26 participants (17 CU, 5 MCI, and 4 aDem).

†The amyloid and tau PET measures are derived meta-ROIs. The amyloid PET meta-ROI includes the prefrontal, orbitofrontal, parietal, temporal, anterior and posterior cingulate, and the precuneus. The tau PET meta-ROI includes the amygdala, entorhinal cortex, fusiform, parahippocampal, and inferior temporal and middle temporal gyri. Abnormal was defined as ≥ 1.48 SUVR for amyloid PET and ≥ 1.25 SUVR for tau PETCU = cognitively unimpaired; MCI = mild cognitive impairment; aDem = amnestic dementia; MCSA = Mayo Clinic Study of Aging; ADRC = Alzheimer's Disease Research Center; SUVR = standardized uptake value ratio; IQR = interquartile range.

Table 2:

Variance components analysis. Values shown are estimates of the SD from between-region, between-participant, and error components.

Variance component	Susceptibility[*]	Amyloid PET[†]	Tau PET[†]	Volume[‡]
Cortical regions				
Region	0.0016	0.07	0.04	0.77
Participant	0.0011	0.22	0.16	0.12
Error	0.0020	0.08	0.07	0.08
Deep and inferior gray regions				
Region	0.041	0.16	0.11	
Participant	0.012	0.12	0.11	
Error	0.018	0.11	0.06	

[*]Expressed in ppm.

[†]Expressed in log SUVR units.

[‡]Expressed as log cm^3.